E-ISSN: 2709-9423
P-ISSN: 2709-9415
JRC 2023; 4(1): 56-68

www.chemistryjournal.net
Received: 19-11-2022
Accepted: 25-12-2022

Pradeep Kumar Vishwakarma
Department of P.G. Studies and Research in Chemistry and Pharmacy, Rani Durgavati Vishwavidyalaya, Jabalpur, Madhya Pradesh, India

Ram Charitra Maurya
Department of P.G. Studies and Research in Chemistry and Pharmacy, Rani Durgavati Vishwavidyalaya, Jabalpur, Madhya Pradesh, India

Correspondence
PK Vishwakarma
Department of P.G. Studies and Research in Chemistry and Pharmacy, Rani Durgavati Vishwavidyalaya, Jabalpur, Madhya Pradesh, India

Experimental and theoretical studies of MoO_2(II) complexes based on pyrazoline and hydrazone derived Schiff base

Pradeep Kumar Vishwakarma and Ram Charitra Maurya

DOI: https://doi.org/10.22271/reschem.2023.v4.i1a.82

Abstract
Both experimental and theoretical chemistry is the preeminent discipline of the chemical sciences. In the striking fascination of this work, we have presented the synthesis and characterization of 4-formyl-3-methyl-1-phenyl-2-pyrazolon-5-one with the isonicotinic acid hydrazide-derived Schiff base H_2L and its cis-dioxidomolybdenum(II) complexes $[MoO_2(L)(CH_3OH)]$ 1 and $[MoO_2(L)(Hbimd)]$ 2 (Hbimd: benzimidazole). Characterization was based on spectral methods, which showed that the complexes exhibit neutral monomeric distorted octahedral geometry. The DFT approach was used for the theoretical study of the compounds. Finally, the compounds were evaluated using the Insilco Bioactivity Score and Drug-Likeness using the online server and ADME properties that led to the pharmaceutical chemistry of the compounds. The biological results, both experimental and insilco, are promising for their future use as medicinally relevant compounds.

Keywords: MoO_2(II), spectroscopy, DFT, and ADME

Introduction
Molybdenum is the only second-row transition metal required by most living systems and is found almost everywhere in biology [1]. Molybdenum represents a critical trace element involved in the structure of specific enzymes and the catalysis of redox reactions [2]. The coordination compounds of this metal play an important role in the treatment of Wilson's disease [3] and hyperglycemia [4] and also show potent anticancer activity [5]. Later, this class of compounds received great interest [6-9].
Recently, quantum chemistry-based structural analysis has become an acceptable and reliable technique. For compounds where X-ray crystal growth fails, computational chemistry-based molecular modelling is the means that can validate experimental observations well. Considering molecules ranging from micro to macromolecules and implying different chemical fronts saves time and labour to obtain the best possible results. Therefore, DFT is described as a powerful approach to predicting the geometrical properties of molybdenum complexes [10]. Theoretical studies have been of great benefit in determining the molecular, electronic, and binding energies of molybdenum complexes at a relevant level of theory [11]. Such studies have led to new insights into organomolybdenum chemistry [12].
Motivated by the applied aspects of cis-dioxomolybdenum complexes, the present study involves a comparative experimental and theoretical investigation of cis-dioxomolybdenum complexes containing Schiff bases of pyrazoline and hydrazone together with benzimidazole as co-ligands. The experimental DFT and insilco ADME activity of the complexes represent the main objective of the work.

Experimental
Material and Methods
All reagents and solvents were commercially available and of quality AR grade. Elemental and NMR spectral analyses were obtained from CDRI, Lucknow. IR Spectra were recorded with Bruker αT FT-IR spectrophotometer using KBr pallets, UV-Vis absorption studies were carried out with Varian Carry 5000, UV/Vis/NIR spectrophotometer, electrochemistry was carried out with Epsilon BASi cyclic voltameter using TBAP as supporting electrolyte and decomposition temperature was monitored with an electrically operated melting point apparatus with a heating capacity up to 360/ºC from our department.

A theoretical study was performed using the density functional theory method (DFT) with B3LYP/LANL2DZ combinations included in the Gaussian 09 software package. The bioavailability of the studied compounds was predicted using the web server www.molinspiration.com.

Synthesis of Schiff base H_2L and its MoO_2(II) complexes 1 and 2

Schiff's base was found by an equimolar methanolic solution of 4-formyl-3-methyl-1-phenyl-2-pyrazolon-5-one (0.204 g) and isonicotinic acid hydrazide (0.137 g) with constant stirring and refluxed for 4 hours. The resulting solution of H_2L precipitates as a yellow solid. The desired compound was filtered, washed several times with methanol, and dried in a desiccator over anhydrous $CaCl_2$. Complex 1 was prepared by refluxing $[MoO_2(acac)_2]$ (0.326 mg, 1 mmol) with H_2L (0.323 g) in methanol, precipitating a crystalline solid after 4 hours. Complex 2 was obtained in the same way as complex 1, but after 3 hours a methanolic solution of benzimidazole (0.118 g) was added and the reaction continued for another 1 hour. The separated crystalline solid was filtered and washed several times with methanol and dried in a desiccator over anhydrous $CaCl_2$.

Result and Discussion

In the current research article, the Schiff base ligand, (4Z,N'E)-N'-((5-hydroxy-3-methyl-1-phenyl-1H-pyrazol-4-yl)methylene) isonicotinohydrazonic acid (H_2L) and its MoO_2(VI) complexes 1 and 2 were synthesized via the following synthetic pathway shown in Scheme 1 and 2, respectively. The synthesis methods are described in the experimental section. The proposed structure and molecular composition were confirmed by numerous analytical methods. The decomposition temperature of the ligand and its complexes was also recorded; the ligand shows 230 °C, while the complexes show 255 and 280 °C, indicating the metal-ligand interactions.

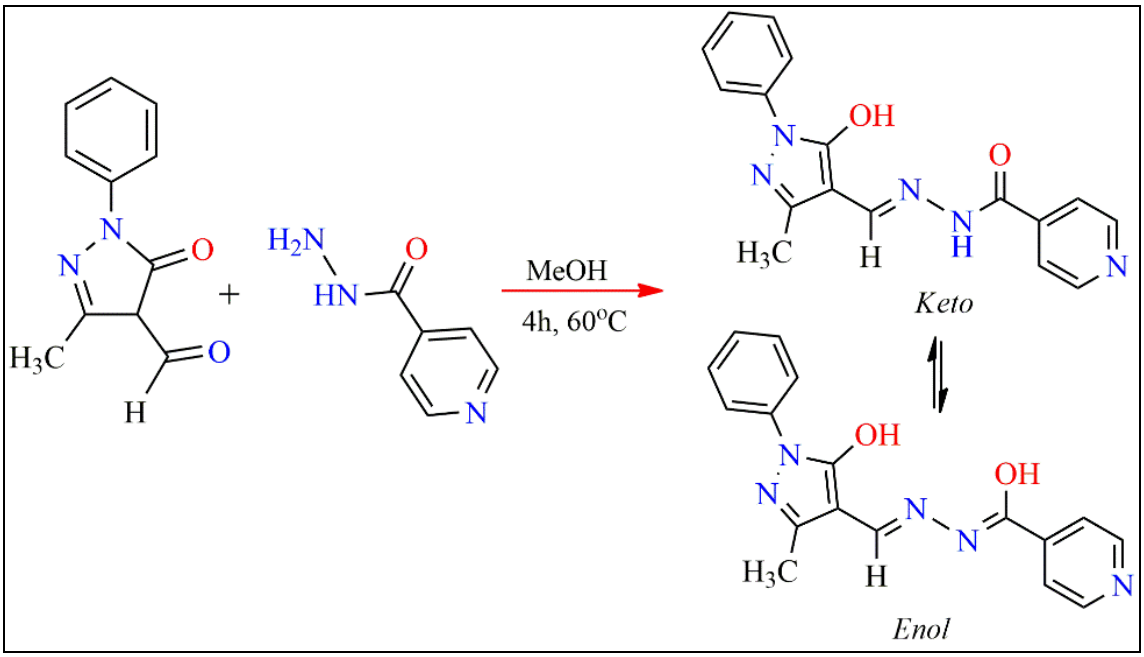

Scheme 1: Synthetic route of Schiff base ligand H_2L.

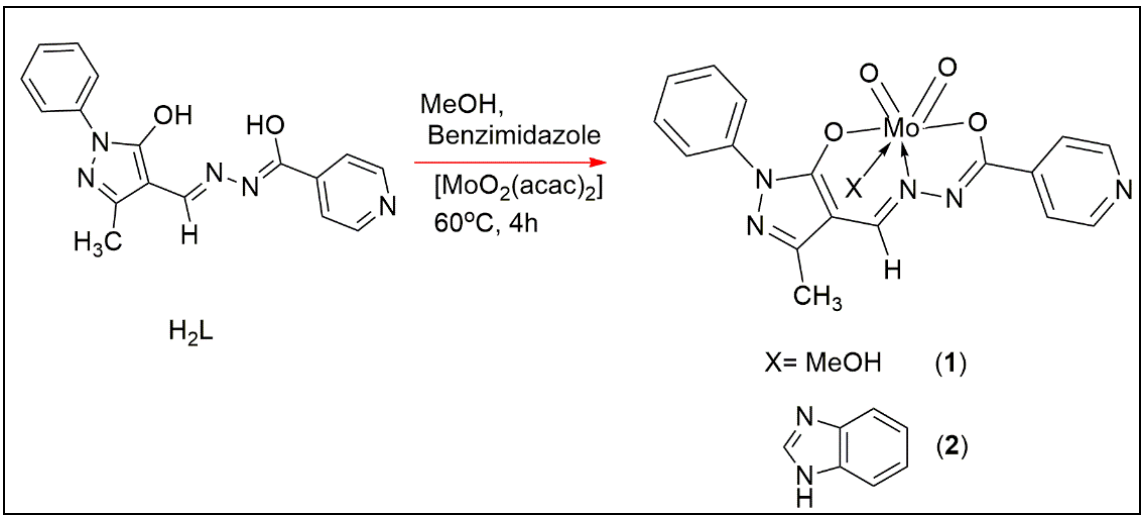

Scheme 2: Synthetic route of MoO_2(VI) complexes **1** and **2.**

FT-IR Spectral Analysis

The validation of the Schiff base synthesis is evident from the FT-IR spectral analysis. The significant vibrational peaks of H2L are shown in Figure 1. The compound shows characteristic spectral bands: a broad band at 3449 cm-1 for ν(O-H), a sharp band at 1585 cm-1 due to ν(C=N), and the peak of ν(C=O) is merged with the azomethine group. The band of ν(N-H) is observed at 3127 cm^{-1}. The above discussion indicates that the ligand in the present studies occurs in the solid state in the keto form; after complexation, the keto form becomes an enol form due to keto-enol tautomerization. The structural details of the ligand, both keto-enol tautomeric forms, are shown in Scheme 1. The infrared spectra of the complexes studied were observed in comparison with the spectrum of the ligand and their assignments are summarised in Table 1. In the IR spectrum of the Schiff base, a characteristic band appeared at 1623 cm-1 due to ν(-N=C). The shift of this band to higher wavenumbers or the blue shift in the spectra of the metal complexes indicates the coordination of the azomethine nitrogen with the metal center [13, 14]. The dioxomolybdenum(VI) complexes show a symmetric and asymmetric band at 905 and 915 cm-1 (O=Mo=O), indicating the presence of a cis-[MoO2] group [15]. The FTIR spectra of the synthesized compounds are shown in Figures 2 and 3. The presence of a broad band centered at ~3400 cm-1 attributed to the ν(OH) mode of water is most likely due to the moisture present in the samples. This is also supported by the fact that no water loss was observed in the thermograms (vide infra), either as lattice or coordinated water in the complexes.

The correlation curve between the experimental and theoretical vibrational frequencies was studied as linear and given by the equations of the corresponding complex 2 [y=0.9765x+43.306 (R2=0.9985)]. The experimental spectra were compared with the calculated spectra of the representative complexes, which are also listed in Table 1. Some minor differences in the frequencies could be due to polarization, calculation effects, and experimental conditions.

Table 1: Selected observed and computed IR frequencies of H_2L and their metal complexes.

Compounds	*ν*(C=N)	*ν*(O-H) / *ν*(N-H)	*ν*(C-O)	*ν*(M-O)	*ν*(M-N)	*ν*(M=O)
H_2L	1586	3429	1327	-	-	-
[MoO_2(L)(MeOH)] 1	1609	3418	1161	571	486	905, 915
[MoO_2(L)(Hbimd)] 2	1614 (1618)	3407	1221 (1230)	591	497	904, 915 (946, 892)

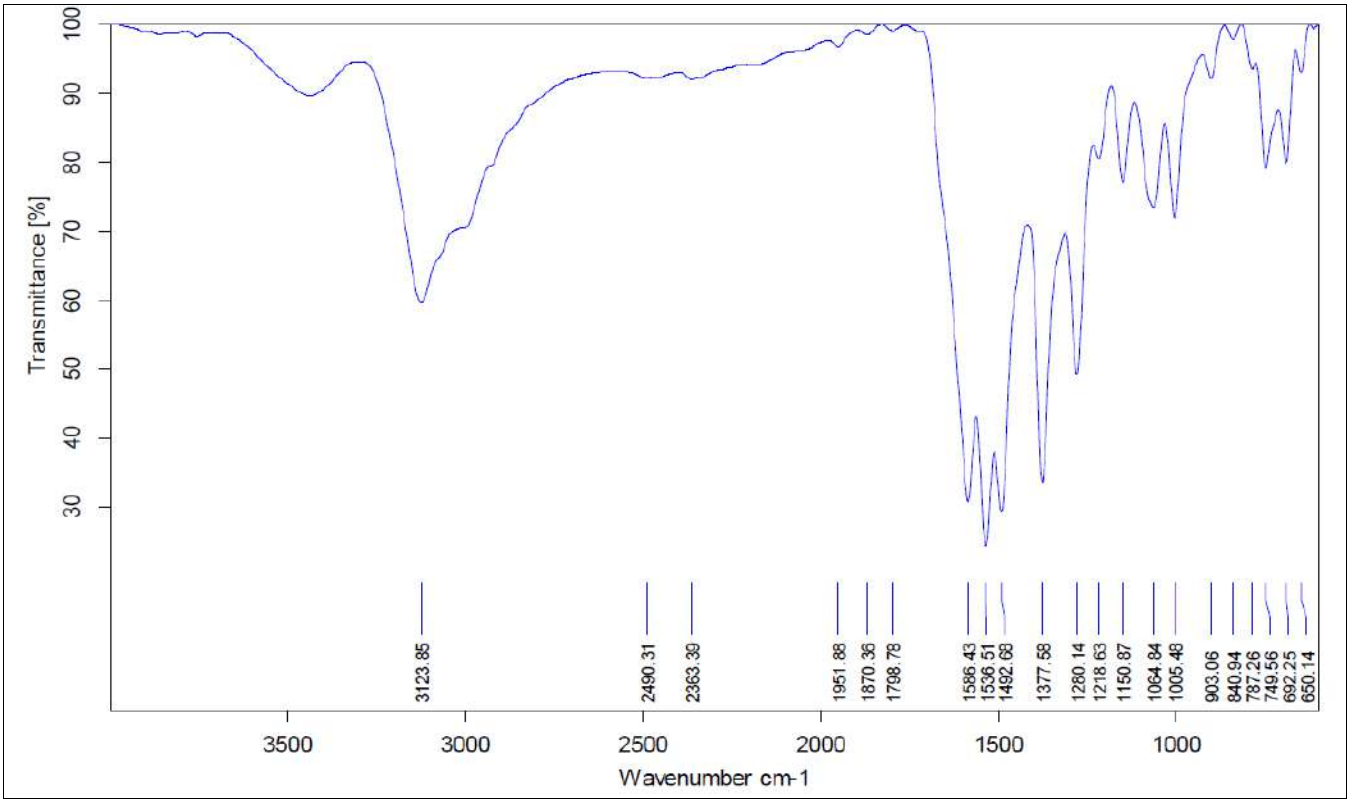

Fig 1: Experimental FT-IR spectrum of H_2L.

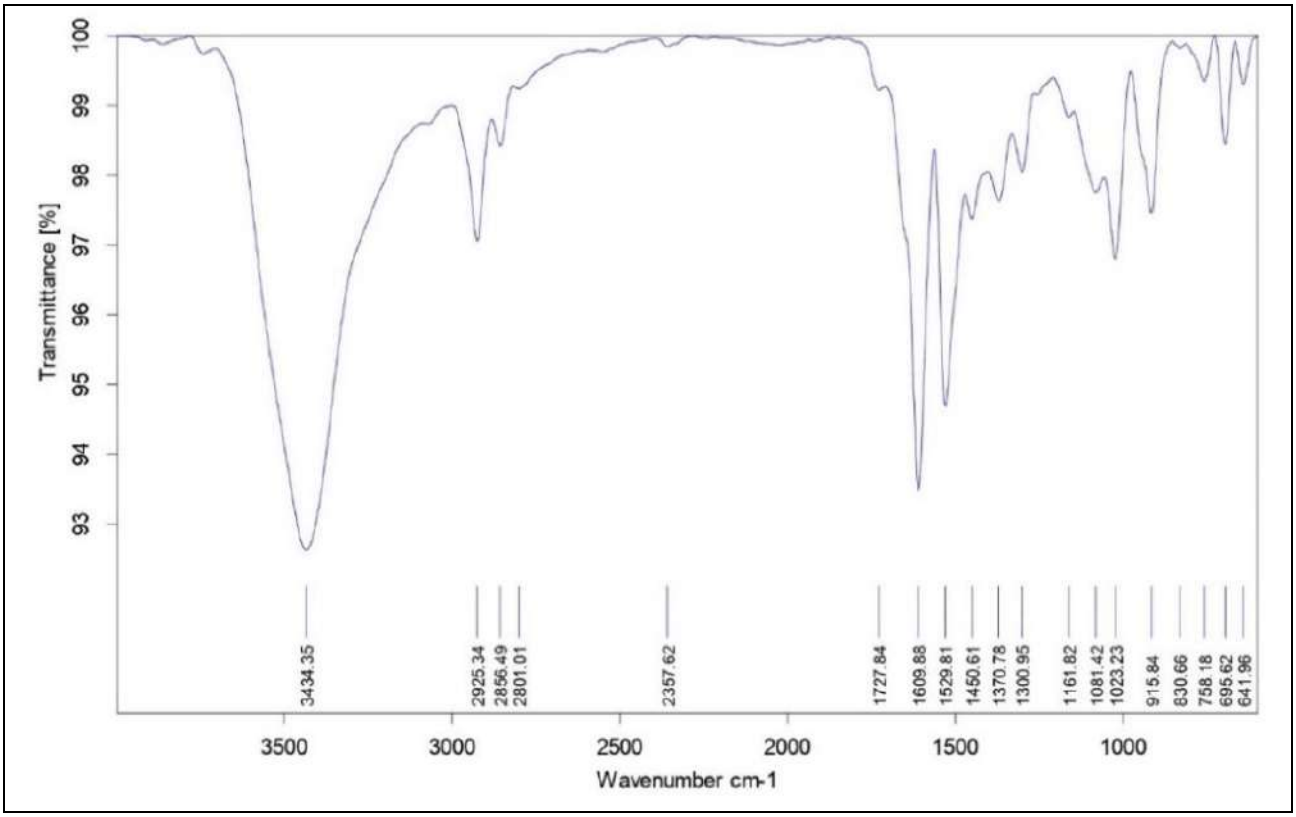

Fig 2: Experimental IR spectrum of **1**.

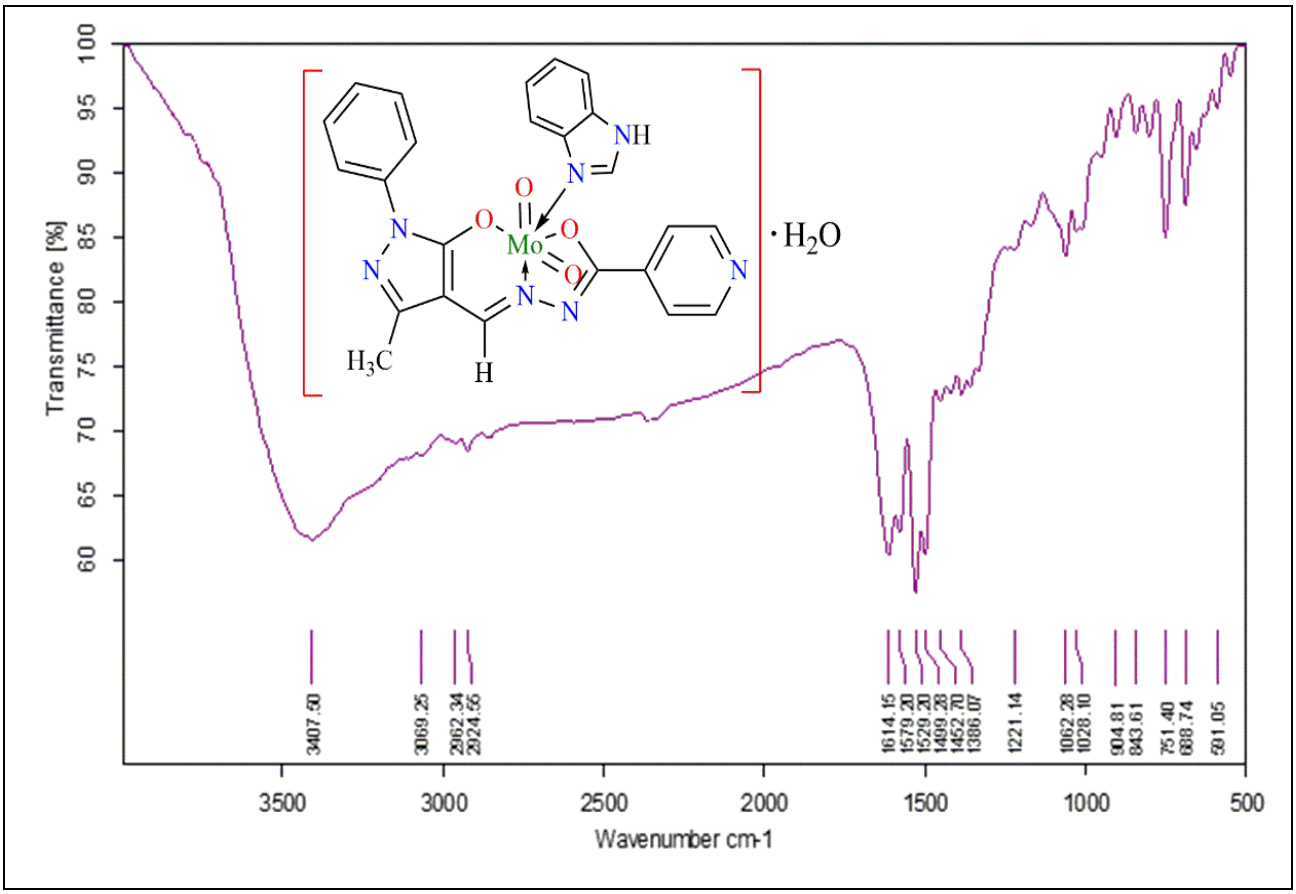

Fig 3: Experimental IR spectrum of **2**.

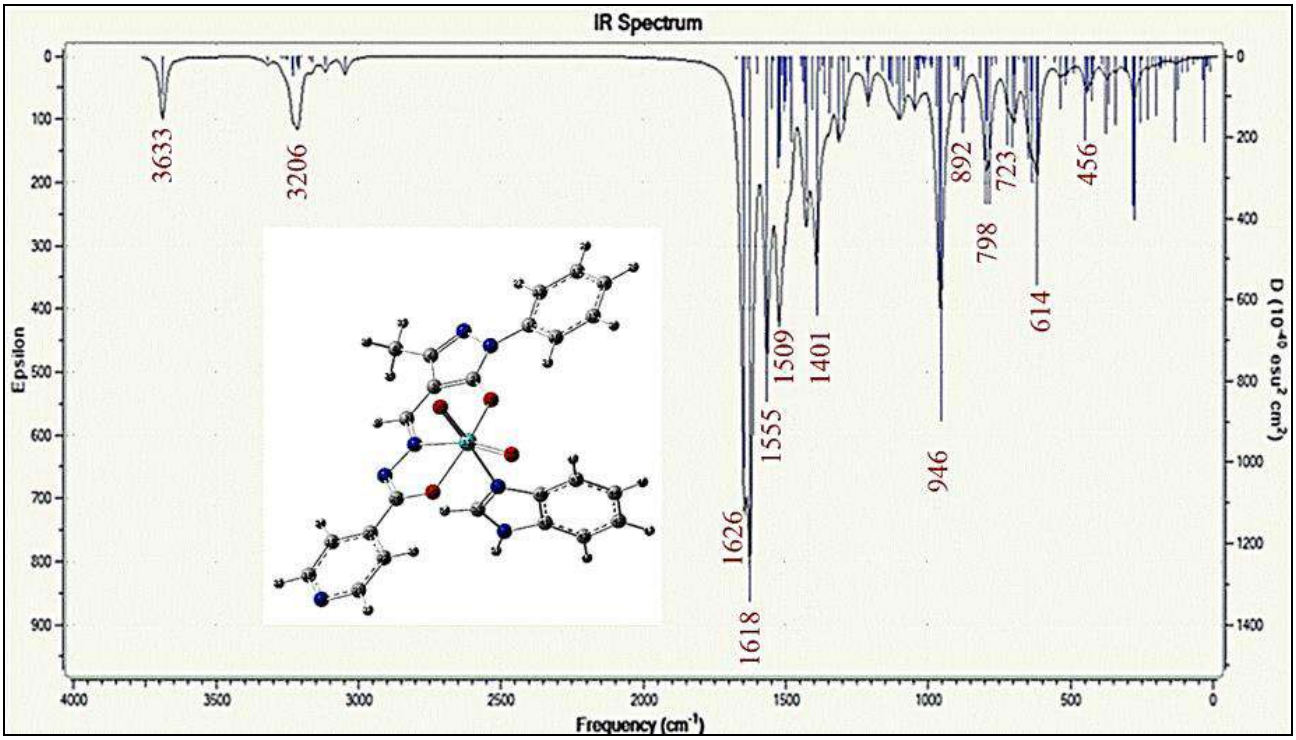

Fig 4: Theoretical IR spectrum of **2**.

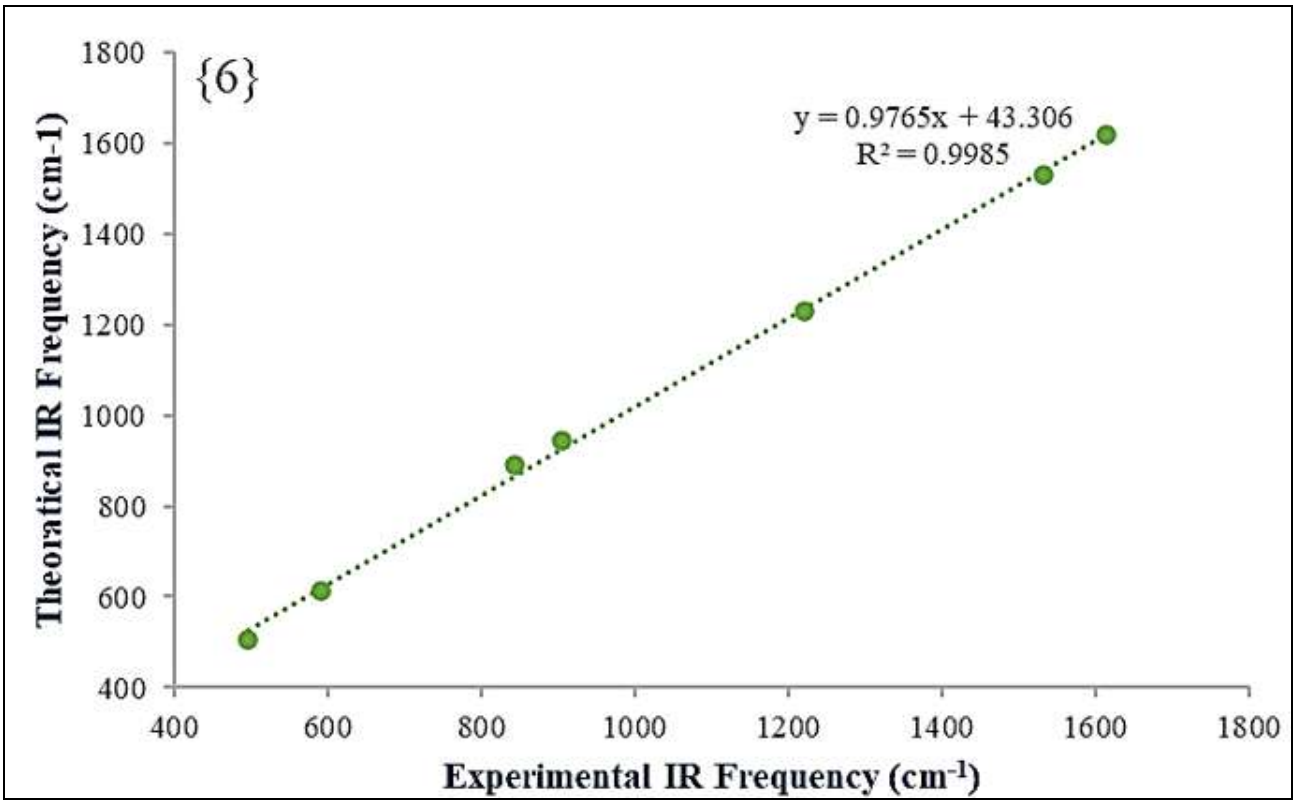

Fig 5: The comparative graph between the experimental and theoretical IR of **2**.

NMR Analysis

In addition to the microanalytical analysis and infrared spectral studies, the NMR spectra also confirmed the Schiff base synthesis. The ^{1}H-NMR spectra of the Schiff base H_2L and its corresponding complex 1 were recorded in DMSO-d6 (ppm) and are shown in Figures 6 and 7. The Schiff base showed signals at δ 11.3 (s, 1H, - OH), δ 7.1 (d, 1H, -H-C=N) attributed to the resonance of the H-C=N group, hydrogen was assigned as a doublet signal, δ 6.3 (s, 1H, -NH) and δ 2.3 (s, 3H, H3C-C). Aromatic-H signals were observed at δ 7.2-7.8 ppm. [MoO2(L1)(MeOH)] 1 showed signals at δ 8.7 (d, 1H, -H-C=N), δ 1.92.3 (s, 3H, H3C-C), and the aromatic-H signals were observed at δ 7.2-7.8 ppm. Moreover, the signal at δ = 3.86 ppm was attributed to the OCH_3 group [16] of methanol, which was due to the coordination with the metal center. In the ^{1}H-NMR spectrum, the H_2L singlet appeared at δ 11.3 due to the - OH proton disappearing in the spectrum of the complex,

indicating coordination by the oxygen atom with the metal ion. A sharp singlet peak in the ligand at δ = 6.3 ppm is the free N-H group, and again the absence of this signal in the complex supports the conclusion from the IR spectral studies, i.e., the enolization of the keto group followed by its coordination.

Table 2: ^{1}H-NMR chemical shift data and their assignments of H_2L and 1.

H_2L	1	Assignments
11.3	-	O-H(a)
7.2-7.8	7.4-7.8	Ar-H
6.3	-	H-N-C(b)
7.1	8.7	H-C=N(c)
2.3	1.9	H_3C-C(d)
2.5	2.5	DMSO(*)
-	3.4	H_3C-O(e)

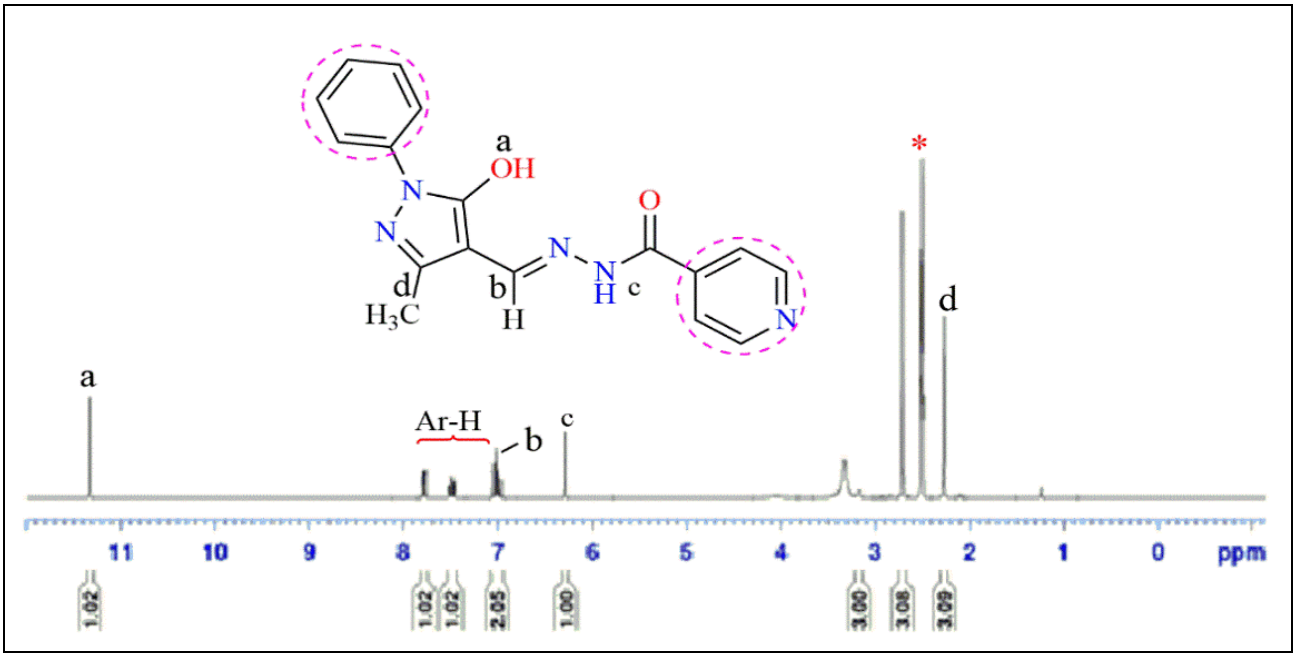

Fig 6: The ^{1}H-NMR spectrum of **H_2L.**

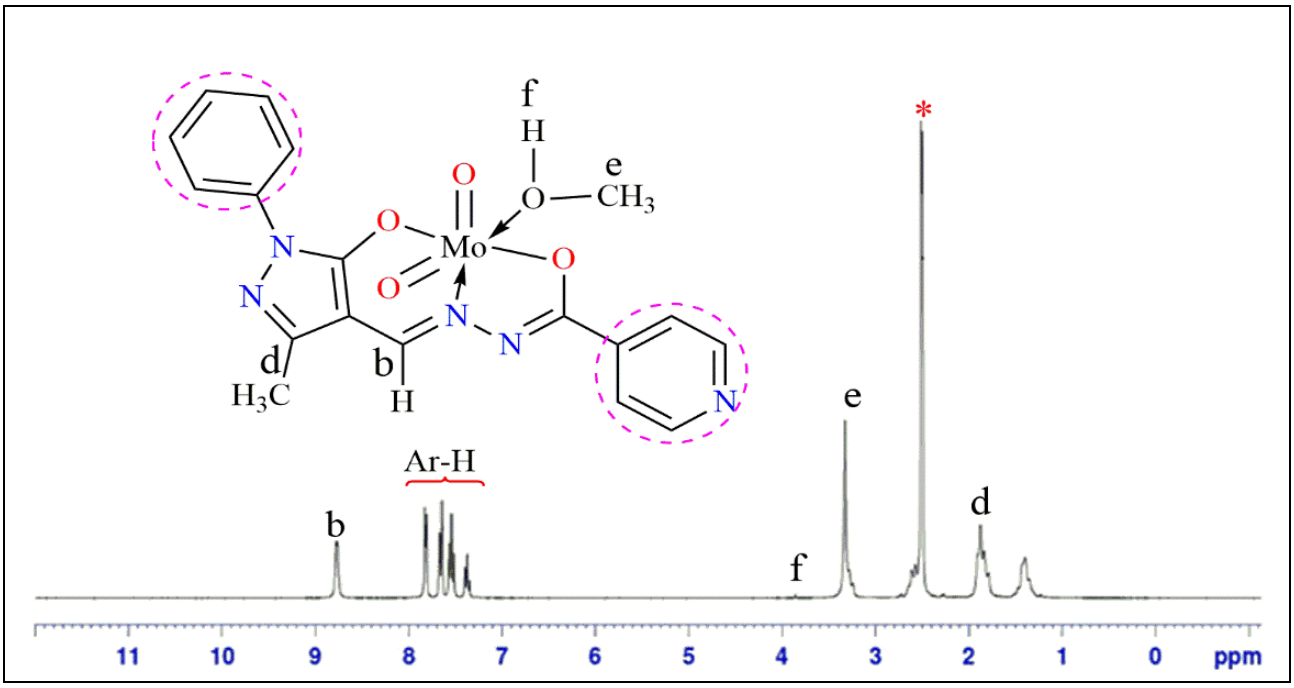

Fig 7: The ^{1}H-NMR spectrum of [MoO_2(L)(MeOH)] **1**.

Electronic Spectral Analysis

The electronic spectral studies of the H_2L and the corresponding complex were recorded in DMSO solution and are shown in Figures 8 and 9, respectively. The ligand H2L exhibits spectral absorption bands at 250 and 356 nm in the UV region due to π-π* and n-π* transitions, respectively [17, 18]. In the electronic spectra of the studied MoO_2(II) complexes, all these bands appear with slight variations in their λmax values. Moreover, an additional band of medium intensity in all complexes at 380-422 nm can be assigned to a ligand-metal charge transfer band [19], which is due to the charge transfer from the filled p-orbitals of the coordinated enolate oxygen atoms to the empty d-orbitals of the metal [20].

The theoretical electronic spectrum of compound 2 was calculated by the TD-DFT method with the solvent model using DMSO as solvent at the B3LYP/LANL2DZ theory level and is shown in Figure 10. The compound shows a singlet state due to paired electrons; the compound mainly shows three transition energy bands between HOMOs at 590, 516, and 482 nm. As the experimental spectrum of the molybdenum complex. The lower bands are due to ligand-internal n→π*/π→π* transitions, while the higher bands are most likely due to the ligand-metal charge transfer (LMCT) transitions. The band that did not appear in the far visible region indicates that the d-d transition does not occur in the molybdenum complexes.

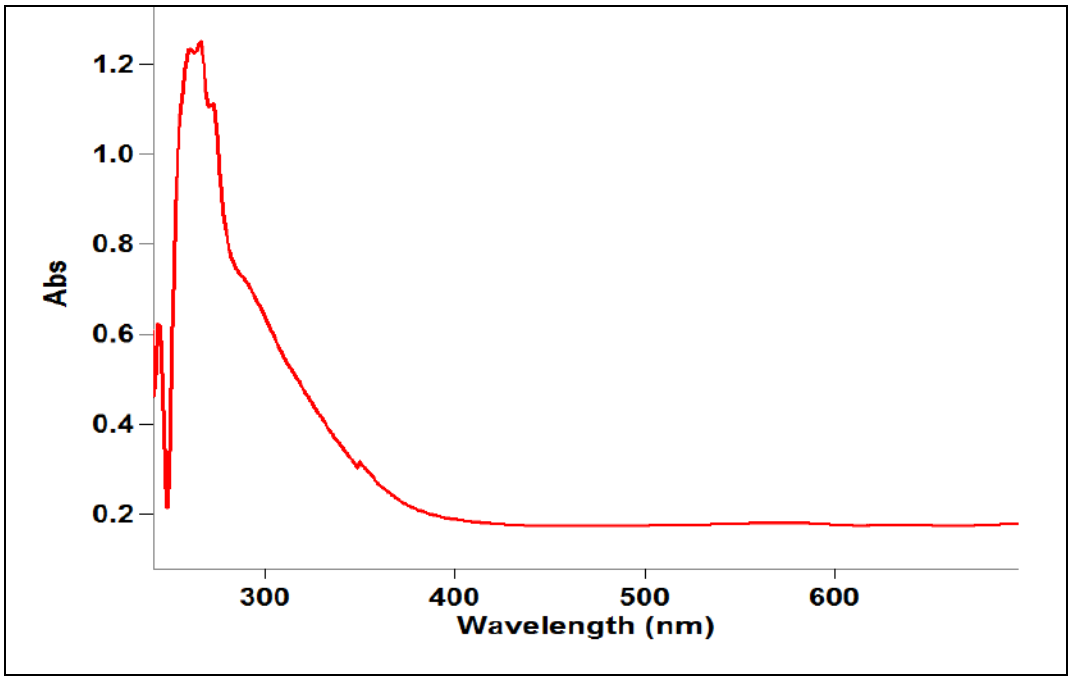

Fig 8: UV/Vis. Spectrum of H_2L in 100 µM DMSO Solution.

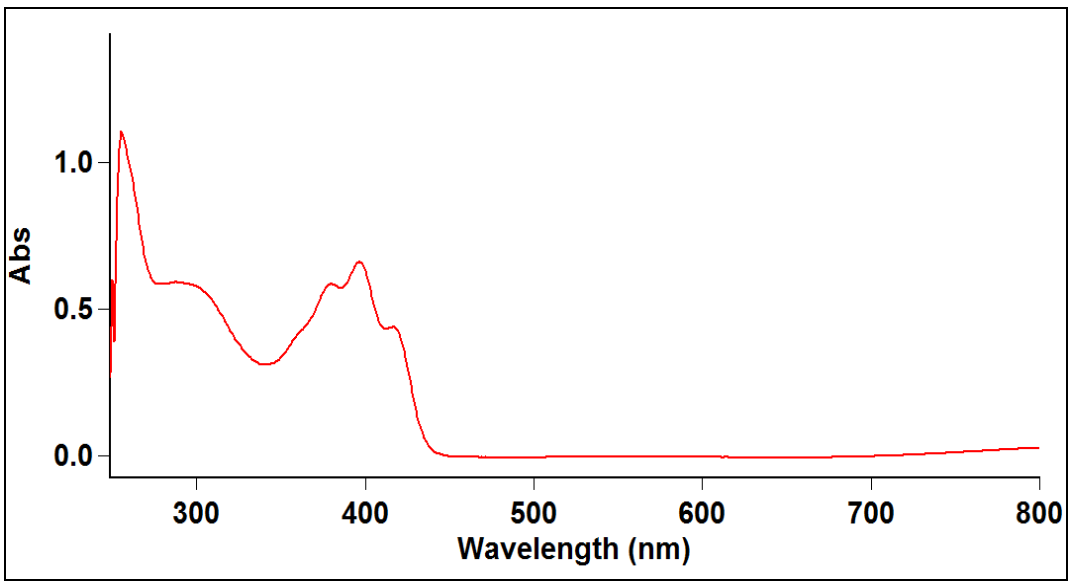

Fig 9: Experimental UV/Vis. spectrum of [MoO_2(L)(Hbimd)] **2.**

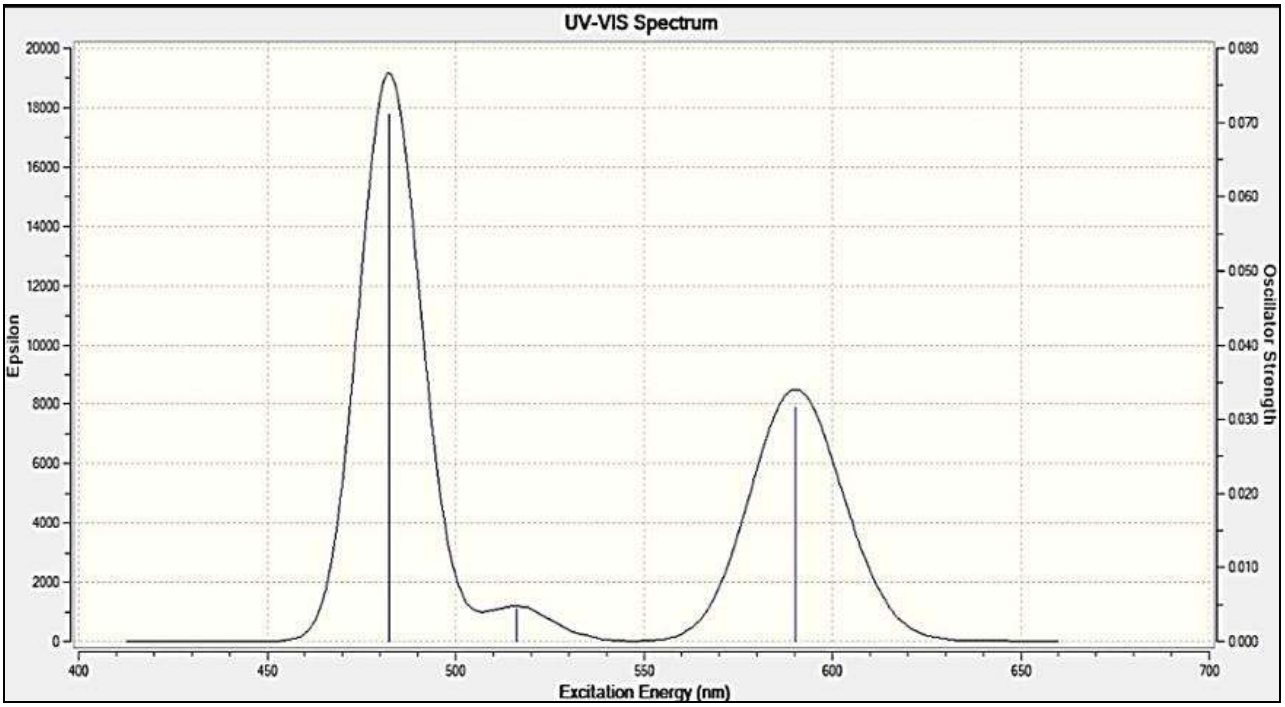

Fig 10: Theoretical UV/Vis. spectrum of [MoO_2(L)(Hbimd)] 2.

Electrochemistry

The electrochemistry of representative complex 2 was monitored in the potential range between ±1,500 V v/s Ag/AgCl in 0.1M solutions of TBAP as an electrolyte in a single scan area. The voltammogram in IUPAC mode is shown in Figure 11. The voltammogram showed two levels of irreversible reduction peaks as [Epc(0.192) and (-0.750) V], and [Ipc (0.210) and (7.115) µA], which can be used to determine $[MoO_2]^{2+}\rightarrow[MoO_2]^{+}\rightarrow[MoO_2]$, and a one-step irreversible oxidation wave as [Epa(-0.622) V] and [Ipa(3.582)]µA], which can be used to determine $[MoO_2]\rightarrow[MoO2]^{2+}$. The corresponding formal reduction potential (E1/2 in V) is -0.688 V. The irreversible redox properties observed for the complexes could be due to the short-lived reduced/oxidized state of the metal ion [21, 22]. Electrochemistry can be associated with FMO studies that significantly affect the formulation of chemical descriptors [23].

The energy of HOMO-LUMO and the energy gap (Eg) were calculated from the Eox (onset) potential and are shown in Table 3. The experimental HOMO-LUMO approximation was performed using cyclic voltammograms and the empirical relationship for EHOMO as [(Eox-E1/2(ferrocene) +4.8] eV. Ferrocene was used as the standard. E1/2(ferrocene) is equal to 0.304 V, which can be used to calculate the energy of HOMO. We can calculate the band gap (Eg) of eV from the electronic absorption spectra 1242/λ (nm). The values of HOMO and LUMO and their energy gap from complex 2 are given in Table 3. While the theoretical chemistry helps to encompass the energy, gap calculated from TD-DFT (ΔE), the energy gap between HOMO-LUMO and complex 2 is 5.069, respectively. Some minor differences in the experimental and theoretical energy gaps could be due to polarization, calculation effects, and experimental conditions. The chemical stability of the molecules is also based on the energy gap between HOMO and LUMO [24, 25].

Table 3: The HOMO-LUMO values from electrochemical and electronic spectral data.

Comp.	E_{ox} V (From CV)	E_{HOMO} eV [E_{ox}-$E_{1/2}$+4.8]	Optical band gap from absorption studies (eV) 1242/λ(nm)	E_{LUMO} (E_{HOMO}-optical band gap)	$E_{HOMO-LUMO}$
2	-0.622	3.874	5.069	-1.195	5.069

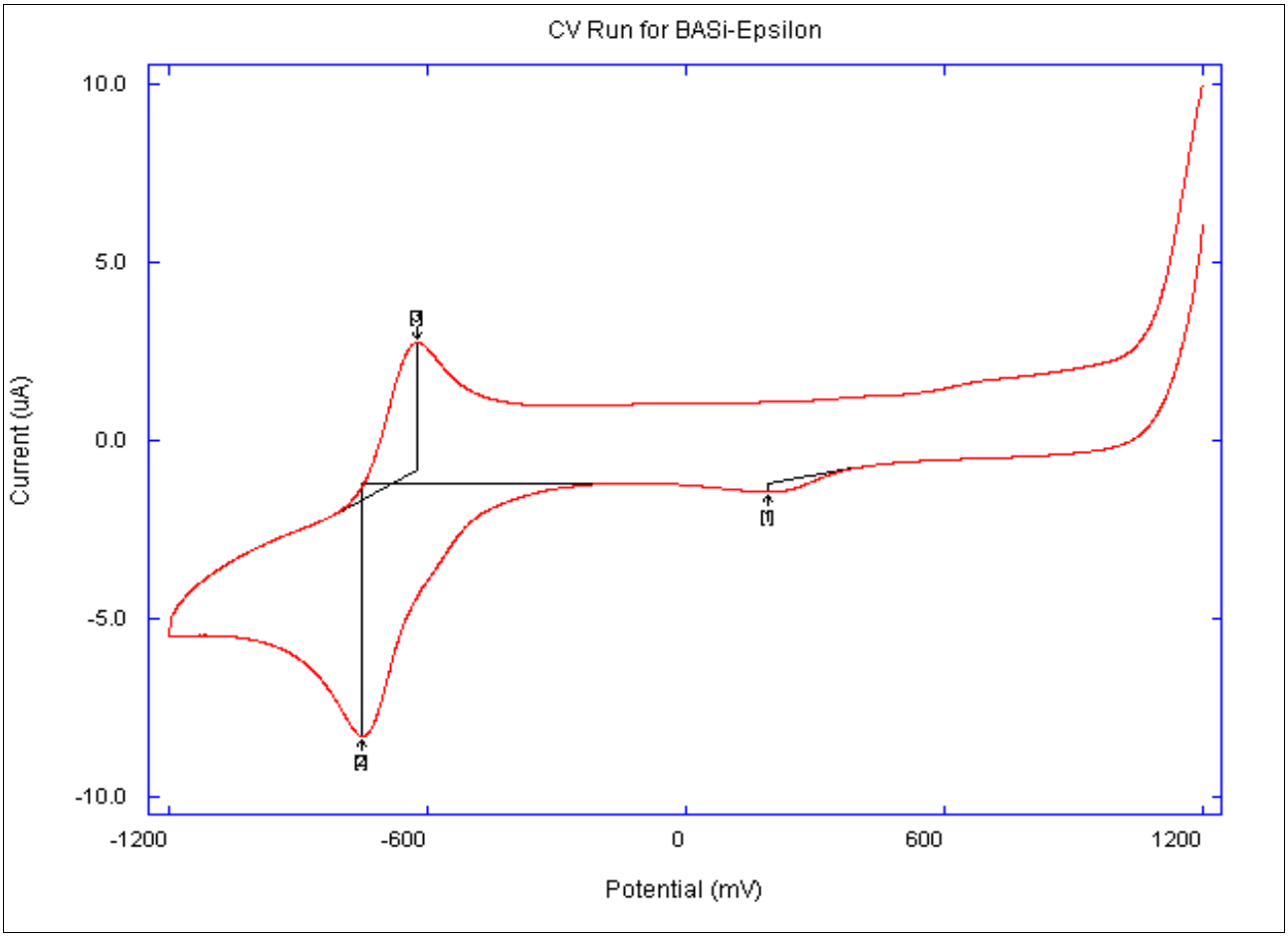

Fig 11: Cyclic voltammograms of complex 2 scan range 100 mV/Sc.

Molecular structural determinations

The molecular geometrical parameters and structural evolutions of the studied complex, namely MoO_2(II) 2, were calculated using DFT. The molecular structures of 2 consist of a tridentate ONO donor Schiff base, a monodentate N-donor benzimidazole ligand, and the MoO2(II) centre in the discrete monomeric form. The compound has six coordination numbers that exhibit a slightly distorted square pyramidal geometry around the Cu(II) centre, as shown in Figure 12. Most importantly, the significant bond angle O=Mo=O 105.866 proves the cis-MoO2 unity of this complex. The bond lengths and angles of other cis-dioxidomolybdenum(VI)complexes are reported [26-28].

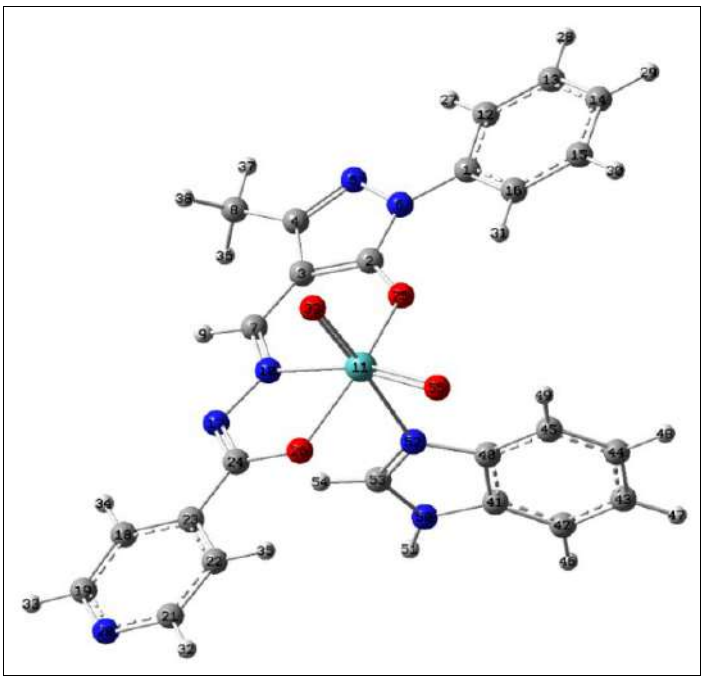

Fig 12: Selected computed geometrical parameters of [MoO_2(L)(Hbimd)] **2.**

Table 4: Selected computed geometrical parameters of [MoO_2(L)(Hbimd)] 2.

Bond Connectivity	(Å)	Bond Connectivity	(°)	Bond Connectivity	(°)
Mo-N(10)	2.307	N(10)-Mo-O(25)	82.841	O(25)-Mo-O(55)	101.115
Mo-O(25)	2.023	N(10)-Mo-O(26)	71.039	O(26)-Mo-O(39)	97.984
Mo-N(26)	2.010	N(10)-Mo-O(39)	90.656	O(26)-Mo-N(52)	82.432
Mo-O(39)	1.734	N(10)-Mo-N(52)	79.430	O(26)-Mo-O(55)	100.085
Mo-N(52)	2.427	N(10)-Mo-O(55)	161.403	O(39)-Mo-N(52)	169.401
Mo-O(55)	1.738	O(25)-Mo-O(26)	154.549	O(39)=Mo=O(55)	105.866
C(7)=N(10)	1.322	O(25)-Mo-O(39)	95.623	N(52)-Mo-O(55)	84.410
		O(25)-Mo-N(52)	79.548		

FMOs Analysis

Analysis of frontier molecular orbitals (FMOs) is an effective approach of DFT electronic interpretation method to determine the interactions between two species, the donor as well as acceptor orbitals. The acronyms stand for the highest occupied molecular orbital [HOMO: H] and the lowest unoccupied molecular orbital [LUMO: L]. The orbitals below these are called NHOMO (next highest occupied molecular orbital) and SLUMO (second lowest unoccupied molecular orbital). These are also commonly referred to as HOMO -1 and LUMO+1. This analysis reveals a crucial feature for the complexation behavior and determination of the reactivity of the molecule. The molecular properties such as reactivity, kinetic stability, chemical potential, optical polarizability, softness-hardness, and electrophilicity were determined by FMO analysis [29-31]. In connection with this, we have used here six molecular orbitals (MOs) inspected for the corresponding studied compound 2. The isosurface contour plots of the FMOs and their energy spacings are calculated directly and shown in Figure 13, and their values are summarized in Table 5. Compound 2 EH is localized over the Schiff base unit and EL is a localized donor atom to the MoO_2(II) center. The electrophilic and nucleophilic nodes are shown as sandwich interactions, these complex molecules and their FMOs are mostly π-antibonding type orbitals. For a better understanding of the FMOs, some functional quantum chemical parameters were calculated using Koopman's theorem [32] as follows and shown in Table 5. The hardness of the molecule is $\eta = (I–A)/2$

(a) The electro negativity of the molecule is $\chi = (I+A)/2$
(b) The chemical potential of the molecule is $\mu = -(I+A)/2$
(c) The softness of the molecule is $S = 1/2\eta$
(d) The electrophilicity index of the molecule is $\omega = \mu^2/2\eta$

Where (A) is the ionization potential and (I) is the electron affinity of the molecule. I and A can be expressed by the energies of the H (HOMO) and L (LUMO) orbitals as I = - EH and A= - EL. The energy gap ΔE defines the softness and hardness of a molecule, if a molecule has a large energy gap, the molecule is hard and soft molecules have a small energy gap [33]. There is a very short energy gap of 3.133 eV.

Table 5: Quantum chemical descriptors based on FMOs analysis.

Comp.	E_{HOMO}	E_{LUMO}	ΔE	η	χ	μ	S	ω
MoO_2 2	-6.233	-3.132	3.101	-1.550	-4.682	1.550	-0.322	-0.775

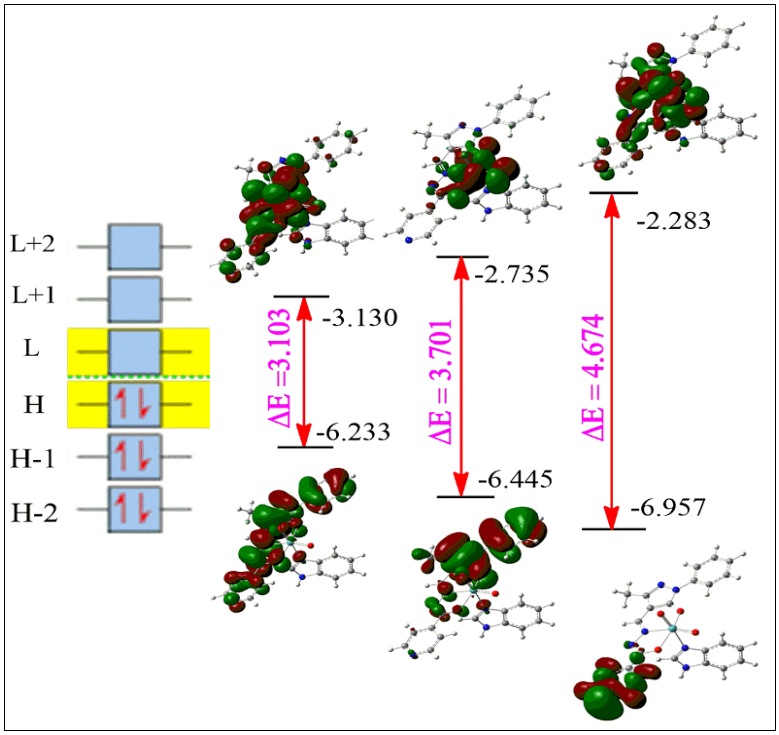

Fig 13: HOMO-LUMO Plot with energy level diagram of MoO_2 complex 2.

Insilco Biological Prediction

Bioactivity ranking prediction of drug-likeness properties

The pharmacological activity of drug molecules is well defined by their highly applicable interaction with a variety of biological targets, including enzymes, ion channels, and receptors in living systems. The bioavailability of the studied compounds was predicted by calculating them via the web server www.molinspiration.com; the results are shown in Table 5. Bioactivity values are monitored based on the following five parameters: (i) G-protein-coupled receptor ligand (GPCRL), (ii) Ion channel modulation (ICM), (iii) Nuclear receptor ligand (NRL), (iv) Protease inhibition (PI), (v) Enzyme inhibition (EI), Based on previous research, substances with bioactivity values of 0.0 or higher are extremely bioactive, while those with values of 5.0 to 0 have moderate activity and those with a value of 5.0 or higher are inactive [34]. The compounds studied here have values from -0.88 to -0.01, so they are expected to have moderate activity. Predictably, they will retain such properties, which require them to be potential drugs with some changes in their molecular structure [35].

The key point for the chemistry of drug design and its development is Lipinski's Rule of Five (RO5). This helps describe molecular features of pharmaceutics that provided insight into many pharmacokinetic parameters, including absorption, distribution, metabolism, and excretion (ADME), for predicting the success of an orally administered drug's journey through the body to the site of action. Via a certain molecular characteristic, (i) logP (partition coefficient), (ii) molecular weight, (iii) multiple hydrogen bond acceptors, (iv) hydrogen bond donors, and (v) polar surface area, the rule predicts the oral activity of a drug. According to RO5, an active ingredient for an orally active drug should have a logP (≤5), hydrogen bond acceptors (≤10), hydrogen bond donors (≤5), and a molecular weight of (≤500) [36]. An orally active drug should typically have no rule violations. Here, the data for percent absorption of the compound under study, TPSA, mLogP, and other parameters are calculated and summarized in Table 6. According to Lipinski's rule [37], the mLogP values of the studied compounds H2L are 1.59 and those of complexes 1 and 2 are -5.37 and -4.91, respectively. These values are satisfactory for a drug molecule that can penetrate biomembranes and has good bioavailability. The investigated compounds are suitable as oral therapeutic molecules according to RO5. However, recent advances in drug discovery have expanded the chemical space for orally administrable candidates beyond the Lipinski rule. Therefore, the investigated compounds can be considered as oral therapeutic molecules according to RO5. However, recent advances in drug discovery have expanded the chemical space for orally administrable candidates beyond Lipinski's rule of 5 (bRo5) by considering the interaction with the target molecule and incorporating various natural products with high activity [38].

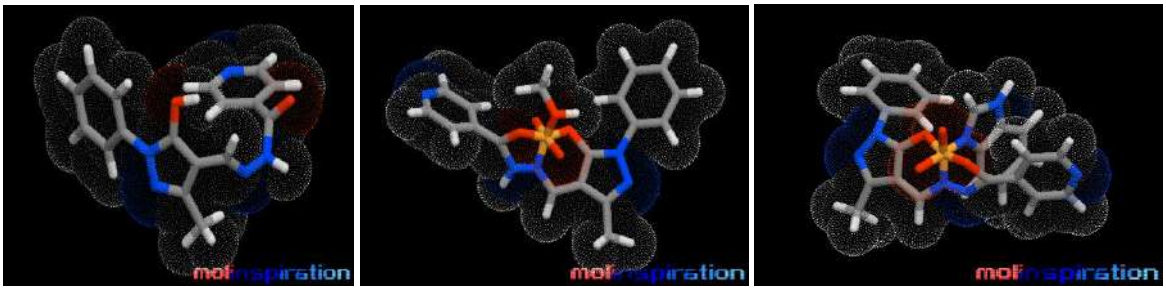

H_2L 1 2

Fig 14: 3D-Molecular structures of ligand studied ligand and their metal complexes obtained through Molinspiration galaxy 3D structure generator v2021.01 beta a web-tool.

Table 5: Bioactivity score of the synthesized ligands and their metal complexes.

Comp.	Parameters of Bioactivity Score					
	GPCR ligand	Ion channel modulator	Kinase inhibitor	Nuclear receptor ligand	Protease inhibitor	Enzyme inhibitor
H_2L	-0.43	-0.47	-0.42	-0.88	-0.62	-0.44
1	-0.06	-0.04	-0.06	-0.38	-0.15	-0.06
2	-0.05	-0.01	-0.12	-0.64	-0.17	-0.04

Table 6: Bioactivity score of the synthesized ligand and their complexes 1 and 2.

Comp.	Lipinski's Parameters						
	% Abs.	TPSA (Å)^2	mlogP	nOHNH	nON	nrtb	Lipinski's violations
H_2L	77.20	92.41	1.59	2	7	4	0
1	69.45	114.63	-5.37	2	10	3	0
2	68.16	118.37	-4.91	1	11	3	2

Percentage absorption (% abs.) was calculated by % Abs = 109-[0.345 × TPSA], Topological polar surface area (TPSA) (defined as a sum of surfaces of polar atoms in a molecule), Logarithm of compound partition coefficient between n-octanol and water, Hydrogen bond donors (nOHNH), Hydrogen bond acceptors (nON) and Number of rotatable bonds (nrotb).

ADMET Prediction

Here, another computerized program is used to evaluate

ADME properties. This work was performed to investigate whether the compounds produce toxicity or exhibit pharmacokinetic contours after administration in the body. The ADMETSAR method [39] was used for this purpose (http://lmmd.ecust.edu.cn/admetsar2). This study is based on the molecular structure of the desired compounds characterized for the prediction of their pharmacokinetic properties such as absorption, distribution, metabolism, and elimination (ADME) as well as their pharmacodynamic potential and toxicity behavior to avoid possible drug interactions with anti-targets that cause many side effects. Different absorption and excretion models are used, namely (i) water solubility (LogS), (ii) Caco-2 cell permeability, (iii) blood-brain barrier (BBB) penetration, (iv) human intestinal absorption (HIA) and toxicity parameters such as (i) carcinogenic, (ii) LD50 dose, etc. The output ADMET data of the compound under study are shown in Table 7. The ADMET properties express that the compounds have high absorption and distribution properties as evidenced by the higher values for HIA, the BBB, and the Caco2 permeability, suggesting promising pharmacokinetic properties. The carcinogenic profile also showed a noncarcinogenic character. An important piece of information from ADMETSAR is the calculated median lethal dose (LD50) in the rat model (acute rat toxicity), which helps in deciding the lethality of compounds. The lower the LD50 value, the more lethal the compounds are compared to those with higher LD50 values. The LD50 values of the compounds studied are mostly higher than those of the commonly used drug streptomycin (LD50=1.841 mol/kg).

Table 7: ADMET activity score of the Schiff base ligand and complexes.

Comp.	BBB	HIA	Caco2	ROCT	Carcinogenicity	LogS	LD50 mol/kg
H_2L	0.915	0.990	0.537	Non-inhibitor	Non-carcinogens	-2.432	2.229
1	0.545	0.909	0.603	Non-inhibitor	Non-carcinogens	-3.406	2.586
2	0.896	0.904	0.554	Non-inhibitor	Non-carcinogens	-3.595	2.568

Blood-Brain Barrier (BBB), Human Intestinal Absorption (HIA), Caco-2 Permeability (Caco-2) and Renal Organic Cation Transporter (ROCT) (LogS) Aquas solubility.

Conclusions

The synthesized compounds have been formulated from the experimental and theoretical investigations, it is confirmed that the target ligand is diprotic tridentate nature and complexes are monomeric and nature. In this series, the DFT approach provides predict the geometry of the metal complexes that have distorted octahedral geometry. Comparison between calculated values of various structural, electronic, and spectroscopic parameters. Theoretical results are in agreement with the experimental results. Additionally, computational FMOs analyses investigated the studied compound. In addition to the synthesis and formulation of studies compounds, several biological assets' computational and experimental activity was assessed. Good pharmacokinetics and biological activity are credited with the insilco biological outcomes.

Acknowledgments

We are thankful to our honorable Vice-Chancellor, Prof. Kapil Deo Mishra, and head of the department Prof. P.K. Khare for encouragement and motivation. I also acknowledge SAIF, CDRI Lucknow for analysis.

Conflict of Interest: None

References

1. Hille R, Hall J, Basu P. The Mononuclear Molybdenum Enzymes. Chem. Rev. 2014;114:3963-4038.
2. Pritsos CA, Gustafson DL, Xanthine dehydrogenase and its role in cancer chemotherapy. Oncol Res. 1994;6(10-11):477-481.
3. Haywood S, Dincer Z, Holding J, Parry NM. Metal (molybdenum, copper) accumulation and retention in brain, pituitary and other organs of ammonium tetrathiomolybdate-treated sheep. Br. J. Nutr, 1998;79(4):329-331.
4. Thompson KH, McNeill JH, Orvig C. Vanadium compounds as insulin mimics. Chem. Rev. 1999;99(9):2561.
5. Waern JB, Harding MM. Bioorganometallic chemistry of molybdocene dichloride. J Organomet Chem. 2004;689(25):4655-4668.
6. Yamase T, Fujita H, Fukushima K. Medical chemistry of polyoxometalates. Part 1. Potent antitumor activity of polyoxomolybdates on animal transplantable tumors and human cancer xenograft. Inorg. Chim. Acta. 1988;151(1):15-18.
7. Rhule JT, Hill CL, Judd DA, Schinazi RF. Polyoxomolybdates in medicine. Chem Rev. 1998;98(1):327-358.
8. Litos C, Terzis A, Raptopoulou C, Rontoyianni A, Karaliota A. Polynuclear oxomolybdenum(VI) complexes of dihydroxybenzoic acids: synthesis, spectroscopic and structure characterization of a tetranuclear catecholato-type coordinated 2,3-dihydroxybenzoate and a novel tridentate salicylato-type coordinated 2,5-dihydroxybenzoate trinuclear complex. Polyhedron. 2006;25(6):1337-1347.
9. Mir JM, Roy S, Vishwakarma PK, Maurya RC. cis-Dioxomolybdenum (VI) complex of N-ohydroxyacetophenonene-isonicotinic acid hydrazide as nosocomial anti-infectious agent: experimental and theoretical study Journal of the Chinese Advanced Materials Society; c2018. https://doi.org/10.1080/22243682.2018.1466727
10. Pandey KK, Patidar P. Theoretical investigation of triple bond in molybdenum complexes *trans*-[$X(PMe_3)_4MoE(Mes)$] (X = F, Cl, Br, I; E = Si, Ge, Sn, Pb): A DFT study. Polyhedron. 2012;37(1):85-93.
11. Pandey KK, Patidar P, Bariya PK, Patidar SK, Vishwakarma R. Assessment of density functionals and paucity of non-covalent interactions in aminoylyne complexes of molybdenum and tungsten [(η^5-C_5H_5)$(CO)_2M{\equiv}EN(SiMe_3)(R)$] (E = Si, Ge, Sn, Pb): a dispersion-corrected DFT study. Dalton Trans. 2014;43(26):9955-9967.
12. Maurya RC, Vishwakarma PK, Mir JM, Rajak DK. Oxidoperoxidomolybdenum(VI) complexes involving

4-formyl-3-methyl-1-phenyl-2-pyrazoline-5-one and some β-diketoenolates. J Therm. Anal. Calorim. 2016;124:57-70.
13. Singh K, Singh DP, Warba MS, Tyagi P, Mirza Y. some bivalent metal complexes of Schiff bases containing N and S donor atoms. J Enz. Inh. Med. Chem. 2006;21(6):749-755.
14. Angelusiu MV, Barbucenau SF, Draghici C, Majan GL. New Cu (II), Co (II), Ni (II) complexes with aroyl-hydrazone based ligand. Synthesis, spectroscopic characterization and *in vitro* antibacterial evaluationEur. J Med. Chem. 2010;45(5):2055-2062.
15. Maurya MR, Tomar R, Gupta P, Avecilla F. Trinuclear *cis*-dioxidomolybdenum(VI) complexes of compartmental C_3 symmetric ligands: Synthesis, characterization, DFT study and catalytic application for hydropyridines (Hps) *via* the Hantzsch reaction. Polyhedron. 2020;186:114617.
16. Karaoglu K, Baran T, Serbest K, Er M, Degirmencioglu I. Two novel macroacyclic Schiff bases containing bis-N_2O_2 donor set and their binuclear complexes: synthesis, spectroscopic and magnetic properties. J Mol. Struct. 2009;922(1-3):39-45.
17. Jaffe HH, Orchin M. Theory and Applications of Ultraviolet Spectroscopy, Wiley, New York; c1962.
18. Maurya MR, Mengesha B, Uprety B, Jangra N, Tomar R, Avecilla F. Oxygen atom transfer between DMSO and benzoin catalyzed by *cis*-dioxidomolybdenum(vi) complexes of tetradentate Mannich bases. New J Chem. 2018;42(8):6225-6235.
19. Dinda R, Sengupta P, Sutradhar M, Mak TCW, Ghosh S. Solution Study of a Structurally Characterized Monoalkoxo-Bound Monooxo-Vanadium(V) Complex: Spontaneous Generation of the Corresponding Oxobridged Divanadium(V,V) Complex and its Electroreduction to a Mixed-Valence Species in Solution. Inorg. Chem. 2008;47(13):5634-5640.
20. Maurya MR, Khurana S, Schulzke C, Rehder D. Dioxo- and Oxovanadium (V) Complexes of Biomimetic Hydrazone *ONO* Donor Ligands: Synthesis, Characterization, and Reactivity, Eur. J Inorg. Chem; c2001, 779.
21. Bond AM, Colton R, Mann DR. Comparison of the $[M(IV)(RR'dtc)_3]^+$ M(III)(RR'dtc)3 and $[M(IV)(Et2dsc)_3]^+$/$M(III)(Et_2dsc)_3$ (M = cobalt, rhodium, iridium; dtc = dithiocarbamate; dsc = diselenocarbamate) redox couples and the reactivity of the oxidation state (IV) complexes in solution and in the gas, phase as studied by electrochemical and mass spectrometric techniques. Inorg. Chem. 1990;29(23):4665-4671.
22. Raja N, Ramesh R. Mononuclear ruthenium(III) complexes containing chelating thiosemicarbazones: Synthesis, characterization and catalytic property. Spectrochim. Acta Part A. 2010;75(2):713-718.
23. Kumar SA, Bhaskar BL. Structural elucidation of antihemorrhage drug molecule Diethylammonium 2,5-dihydroxybenzene sulfonate-an *insilico* approach. IOP Conf. Ser.: Mater. Sci. Eng. 2018;310:012124.
24. Parte MK, Vishwakarma PK, Jaget PS, Maurya RC. Synthesis, spectral, FMOs and NLO properties based on DFT calculations of dioxidomolybdenum(VI) complex. J Coord. Chem. 2021;74(4-6):584-597.
25. Alajrawy OI, Almhmdi AA. Dioxomolybdenum (VI) and oxomolybdenum (IV) complexes with N, O, and S bidentate ligands, syntheses, spectral characterization, and DFT studies. J Mole Struct. 2022;1260:132813.
26. Biswal D, Pramanik NR, Chakrabarti S, Drew MG, Sarkar B, Maurya MR, *et al*. New polymeric, dimeric and mononuclear dioxidomolybdenum (VI) complexes with an ONO donor ligand: crystal structures, DFT calculations, catalytic performance and protein binding study of the ligand. New Journal of Chemistry. 2017;41(10):4116-37.
27. Dinda R, Sengupta P, Ghosh S, Sheldrick WS. Synthesis, Structure, and Reactivity of a New Mononuclear Molybdenum(VI) Complex Resembling the Active Center of Molybdenum Oxotransferases. Eur. J Inorg. Chem. 2003;(2)363-369.
28. Pasayat S, Dash SP, Roy S, Dinda R, Dhaka S, Maurya MR, Kaminsky W, Patil YP, Nethaji M. Synthesis, structural studies and catalytic activity of dioxidomolybdenum(VI) complexes with aroylhydrazones of naphthol-derivative Polyhedron. 2014;67:1-10.
29. Vidhya V, Austine A, Arivazhagan M, Quantum chemical determination of molecular geometries and spectral investigation of 4-ethoxy-2, 3-difluoro benzamide. Heliyon. 2019;5(1):e02365.
30. Murray JS, Sen K. Molecular Electrostatic Potentials, Concepts and Applications, Elsevier, Amsterdam; c1996.
31. Mir JM, Roy S, Vishwakarma PK, Maurya RC, cis-Dioxomolybdenum(VI) complex of N-o-hydroxyacetophenonene-isonicotinic acid hydrazide as nosocomial anti-infectious agent: Experimental and theoretical study. J Chin. Adv. Mater. Soc. 2018;6(3):282-300.
32. Koopmans TA. Ordering of Wave Functions and Eigenenergies to the Individual Electrons of an Atom. Physica. 1934;1:104-113.
33. Pearson PG. The principle of maximum hardness. Accounts of Chemical Research. 1993;26(5):250-255.
34. Venturini A, Gonzalez JA. A CASPT2 and CASSCF Approach to the Cycloaddition of Ketene and Imine: A New Mechanistic Scheme of the Staudinger Reaction. Journal Org Chem. 2002;67(25):9089-9092.
35. Khan T, Dixit S, Ahmad R, Raza S, Iqbal A, Joshi S, *et al*. Molecular docking, PASS analysis, bioactivity score prediction, synthesis, characterization and biological activity evaluation of a functionalized 2-butanone thiosemicarbazone ligand and its complexes. J Chem Bio. 2017;10(3):91-104.
36. Lipinski CA, Lombardo F, Dominy BW, Feeney PJ. Experimental and computational approaches to estimate solubility and permeability in drug discovery and development settings. Adv Drug Deliv Rev. 2001;(1-3)46:3-26.
37. Ammal PR, Prasad AR, Joseph A. Synthesis, characterization, *in silico*, and *in vitro* biological screening of coordination compounds with 1,2,4-triazine based biocompatible ligands and selected 3d-metal ions. Heliyon. 2020;6;6(10):e05144. DOI: 10.1016/j.heliyon.2020.e05144
38. Doak, BC, Kohlberg, J. How Beyond Rule of 5 Drugs and Clinical Candidates Bind to Their Targets. J Med Chem. 2016;59(6):2312-2327.
39. Cheng F, Li W, Zhou Y, Shen J, Wu Z, Liu G, *et al*, J Chem. Inf. Model. 2012;52:3099.